UCLouvain

École polytechnique de Louvain

Numerical study of particle harvesting in pipes

Authors : **Yilgor BAKIRCI**
Supervisors : **Mitiadis PAPALEXANDRIS**
Readers :
Academic year 2025–2026
Master [120] in Mathematical Engineering

Abstract

Particle harvesting is an important step in the pharmaceutical industry, as it directly correlates the yield of the manufacturing process. Granular suspensions are subject to study with the objective to passively harvest the particles it contains. To this end, a numerical simulation implementing a dense granular suspensions in a laminar plane Poiseuille flow is used to determine if the boundary conditions could allow harvesting using the intrinsic properties of the flow. The simulations shows the limit of the algorithm when the *true-slip* boundary conditions is applied.
Keywords :plane Poiseuille flow, granular suspensions, boundary conditions, particle harvesting

Acknowledgements

I would like to thank my supervisor, Professor Papalexandris Miltiadis, who supported and guided me throughout this thesis. I also thank him for his continuous availability and patience.

I would like to thank the University of Louvain for authorizing the ethical use of A.I.

I would like to express my gratitude to my family, friends and lover who believed in me as well throughout this final year.

Contents

1 Introduction

Particle harvesting is an important step in many industrial production processes, particularly in the pharmaceutical industry, as it directly correlates the yield of the manufacturing process. Several techniques have been developed and implemented to achieve particle separation but the efficiency of these techniques remains subpar in some applications. Weak efficiency as such motivates the investigation of alternative approaches.

One promising approach consists in exploiting the phenomenon of shear-induced particle migration in Poiseuille flow channels. When a granular suspension flows through a channel under pressure-driven conditions, interactions between the suspended particles and the surrounding fluid induce particles migration across the channel. Indeed, solid particles tend to migrate away from regions of high shear rate towards regions of lower shear rate which leads to an accumulation of particles towards the centre of the channel. This distribution of particles is the starting point of the segregation approach. This could be exploited for particle harvesting by splitting the channel into three areas to collect the central regions in which the particle concentration is higher.

Developing such an approach requires an accurate description of the flow and of the particle distribution within the channel. Numerical simulations provide a powerful opportunity for investigating these phenomena and for studying the influence of the geometrical parameters on the particle migration. Nevertheless, the predictive capability of a numerical model depends not only on the governing equations used to describe the granular suspension, but also on the boundary conditions imposed at the walls of the channel.

In the context of granular suspension flows, different boundary conditions have been proposed to describe the behaviour of the mixture at the channel walls. Conventional conditions, such as the *no-slip* boundary condition, provide a straightforward description of the mixture velocity at a solid wall. However, their ability to accurately represent the behaviour of solid particles may be questioned as multiple studies demonstrated discrepancies between simulation and reality. It has been documented by numerous studies such as Sochi [2011], Cloitre and Bonnecaze [2017] and et al. [2022] that the solid particles undergo an apparent slip on the surface walls of the channel. This *apparent-slip* boundary condition is dependent on the geometry of the channel and the properties of the mixture of interest.

The objective of this master thesis is to conduct a series of parametric studies with respect to the characteristics of the pipe and the flow conditions to quantity the effects on particle migration.

To achieve this objective, the numerical simulations are performed using a Python code developed within the Louvain School of Engineering. Simulations of steady-state plane Poiseuille flows are conducted for the geometry of interest, and the resulting velocity, granular pressure and granular volume fraction profiles are analysed.

This master thesis is structured into five chapters. The second chapter presents a literature review covering the mathematical background required to derive the governing equations implemented in the numerical model. The third chapter provides a detailed description of the numerical model and its implementation. The fourth chapter presents the results obtained and discusses their implications. Finally, the last chapter summarizes the main findings and presents the conclusions drawn from this work.

2 Litterature review

2.1 Mathematical background

To derive the governing equations describing the Poiseuille flow of dense non-colloidal suspensions, it is first necessary to introduce the theorems and mathematical tools used in the derivation.

2.1.1 Reynolds transport and divergence theorems

Theorem 2.1.1 *Let a scalar function $f(\mathbf{x},t)$ be defined on the domain $\mathcal{V} \subseteq \mathbb{R}^3$ with domain boundary $\delta\mathcal{V}$, the **Reynolds Transport Theorem** states :*

$$\frac{d}{dt}\left(\int_{\mathcal{V}} f(\mathbf{x},t)\, d\mathcal{V}\right) = \int_{\mathcal{V}} \left(\frac{d}{dt} f(\mathbf{x},t)\right)\, d\mathcal{V} + \int_{\delta\mathcal{V}} f(\mathbf{x},t)\mathbf{v}\cdot\mathbf{n}\, d\mathcal{S} \tag{2.1}$$

Where $\mathbf{x}$ is the position vector, t is the time, $\mathbf{v}$ is the velocity of the domain $\mathcal{V}$ (not to be confused with the velocity of material particles in the studied domain $\mathcal{V}$), $\mathbf{n}$ is the normal unit vector, and, $\mathcal{S}$ represents the surface of the domain $\mathcal{V}$.

Theorem 2.1.2 *Let a continuously differentiable on the neighbourhood of $\mathcal{V}$ vector field $\mathbf{f}(\mathbf{x},t)$, the **Divergence Theorem** states :*

$$\int_{\mathcal{V}} \nabla\cdot\mathbf{f}(\mathbf{x},t)\, d\mathcal{V} = \int_{\delta\mathcal{V}} f(\mathbf{x},t)\cdot\mathbf{n}\, d\mathcal{S} \tag{2.2}$$

Leibniz Rule can be generalized for more complex functions and domains instead of its standard form in $\mathbb{R}$. This form of Leibniz rule provides a closed-form expression for the time derivative of an integral evaluated over a time-dependent domain $\mathcal{V}$.

Theorem 2.1.3 *Let a continuously differentiable scalar function $f(\mathbf{x},t)$ be defined on the domain $\mathcal{V} \subseteq \mathbb{R}^3$, the **Leibniz Rule** states :*

$$\frac{d}{dt}\int_{\mathcal{V}} f(\mathbf{x},t)\, d\mathcal{V} = \int_{\mathcal{V}} \left[\frac{df}{dt} + \nabla\cdot(f\,\mathbf{u})\right]\, d\mathcal{V} \tag{2.3}$$

Where $\mathbf{u}$ is the velocity vector associated to the position vector $\mathbf{x}$.

2.1.2 Conservation laws

As explained by Drew and Passman [1999], a mixture is represented by a series of bodies $\mathcal{B}_k$, all of which occupy regions of space simultaneously.
The presence of multiple constituents within a mixture is described through the concept of the *average volume fraction.*

Definition 2.1.4 *Let $b(r, \mathbf{x})$ be a ball of radius r centered at $\mathbf{x}$. Let $\overline{V_k(b(r, \mathbf{x}))}$ be the average volume of component k inside the ball $b(r, \mathbf{x})$ and let $V(b(r, \mathbf{x}))$ be the total volume in ball $b(r, \mathbf{x})$. The average volume fraction is defined as :*

$$\overline{\phi}_k = \lim_{r \to 0} \frac{\overline{V_k(b(r, \mathbf{x}))}}{V(b(r, \mathbf{x}))} \tag{2.4}$$

In the present study the mixture is assumed to be saturated and to consist of two different phases, a granular phase and a fluid phase. The *saturation condition* states that the phases completely occupy the available space. Consequently the sum of their volume fraction satisfies Equation [2.5].

$$\phi_f + \phi_s = 1 \tag{2.5}$$

The subscript s refers to the granular phase while the subscript f refers to the fluid phase.

Conservation of mass

In two-phase granular suspensions, the granular and fluid phases are treated as a single continuum when defining mass and by extension mass density.

Definition 2.1.5 *In a closed space, the amount of mass enclosed in that space stays constant over time. Mass can not be created nor destroyed, it can only be transformed. The balance of mass is defined as :*

$$\frac{d}{dt} \int \underline{\rho}_k \, d\mathcal{V} = 0 \tag{2.6}$$

Where $\underline{\rho}_k$ represents the mass density of body $\mathcal{B}_k$, which is the mass per unit total volume.

As discussed previously, the body $\mathcal{B}_k$ does not occupy the entire spatial domain but only a portion ϕ_k of it. Consequently :

$$\underline{\rho}_k = \phi_k \, \rho_k \tag{2.7}$$

Where ρ_k is mass density of phase k per unit volume of phase k.
By combining Theorems [2.1.1], [2.1.2] and [2.1.3] with Equations [2.6] and [2.7], the following result emerges:

$$\int_{\mathcal{V}} \left(\frac{\partial}{\partial t} \left(\phi_k \, \rho_k \right) + \nabla \cdot \left(\phi_k \, \rho_k \, \mathbf{u}_k \right) \right) d\mathcal{V} = 0 \tag{2.8}$$

Equation [2.8] is a definite integral over any mixture volume, its argument must be equal to zero to satisfy the equality.

$$\frac{\partial}{\partial t} \left(\phi_k \, \rho_k \right) + \nabla \cdot \left(\phi_k \, \rho_k \, \mathbf{u}_k \right) = 0 \tag{2.9}$$

Equation [2.9] is also referred in the literature as the *Continuity Equation.*

Conservation of momentum

Definition 2.1.6 *In a closed system, i.e. a system that does not allow transfer of matter with its surroundings, the total momentum remains constant. The balance of momentum is defined as :*

$$\frac{d}{dt}\int \underline{\rho}_k \mathbf{u}_k \, d\mathcal{V} = \mathcal{F}_k^b + \mathcal{F}_k^s \tag{2.10}$$

Where $\mathcal{F}_k^b$ and $\mathcal{F}_k^s$ respectively represents the body and surface source of momentum to phase k.

The body source of momentum to phase k represents the external contributions to the momentum balance, and, can be modelled using the thermodynamic pressure gradient and a quantity f_k describing the exchange of momentum between phases due to their interactions. The latter quantity is referred by Monsorno et al. [2016] as the interphasial momentum exchange.

$$\mathcal{F}_k^b = \int \left(-\nabla\left(P_k\phi_k\right) + f_k\right) \, d\mathcal{V} \tag{2.11}$$

The negative sign preceding the thermodynamic pressure gradient indicates that the mixture flows from a region of high pressure to a region of low pressure.
The surface source of momentum to phase k describes the internal source of momentum of phase k, and, it can be modelled using the stress tensor of phase k. "The stress tensor Σ_k express the forces exerted on a surface element $d\mathcal{S}$ given by the normal unit vector $\mathbf{n}$ oriented outwards"[1].

$$\mathcal{F}_k^s = \int_{\delta\mathcal{V}} \phi_k \Sigma_k \cdot \mathbf{n} \, d\mathcal{S} \tag{2.12}$$

By applying Theorem [2.1.3] and [2.1.2] respectively to the left-hand side of Equation [2.10] and to the right-hand side of Equation [2.12], and, combining the resulting equations with Equation [2.11] the balance of momentum becomes :

$$\int_{\mathcal{V}} \left(\frac{d}{dt}\left(\underline{\rho}_k \mathbf{u}_k\right) + \nabla \cdot \left(\underline{\rho}_k \mathbf{u}_k \otimes \mathbf{u}_k\right) + \nabla\left(P_k\phi_k\right) - f_k - \nabla \cdot \left(\phi_k \Sigma_k\right) \right) \, d\mathcal{V} = 0 \tag{2.13}$$

The argument used to derive the local form of the continuity equation [2.9] remains valid in this situation. Equation [2.13] is a definite integral over an arbitrary mixture volume, its integrand must be equal to zero to satisfy the equality.

$$\frac{\partial}{\partial t}\left(\phi_k \rho_k \mathbf{u}_k\right) + \nabla \cdot \left(\phi_k \rho_k \mathbf{u}_k \otimes \mathbf{u}_k\right) + \nabla\left(\phi_k P_k\right) = \nabla \cdot \left(\phi_k \Sigma_k\right) + f_k \tag{2.14}$$

2.1.3 Navier-Stokes equations

The Navier-Stokes equations are the baselines of the governing equations used in the numerical model and are formed by the balance of mass [2.9] and momentum [2.14].

[1] From Andreotti et al. [2013]

2.2 Plane Poiseuille flow

The present study investigates a dense non-colloidal suspensions under a laminar plane Poiseuille flow. The plane Poiseuille flow describes a flow occurring between two parallel plates as shown in Figure [2.1].

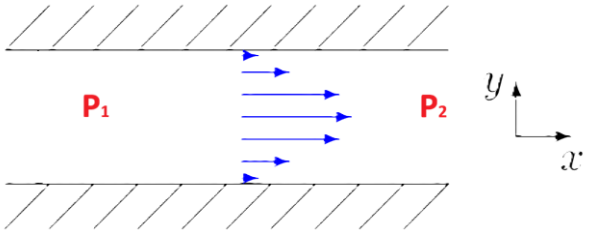

Figure 2.1: Plane Poiseuille flow, $P_1 > P_2$ Borghini [2015]

The plates are located at $y = l$ and $y = -l$ where l denotes the half-width of the channel, the origin is positioned at the centreline of the channel. The pressure gradient and the

2.2.1 Laminar flow

Laminar flow is a fluid flow characterized by low Reynolds numbers Re which indicates low inertia and high viscosity effect. The fluid moves in a smooth and orderly parallel layers with no disruption or mixing between them.

Definition 2.2.1 *The **Reynolds Number** Re is a dimensionless number that characterizes the flow regime, i.e. a **laminar** or **turbulent** flow. The Reynolds number is defined as :*

$$Re = \frac{||\mathbf{u}_f||\, l\, \rho_f}{\mu_f} \tag{2.15}$$

Where $||\mathbf{u}_f||$ represents the magnitude of the velocity of the fluid, l denotes the characteristic length of the system (i.e. the half width of the channel in the plane Poiseuille flow), ρ_f is the density of the fluid and μ_f is the dynamic viscosity of the fluid.

The present study considers a "Reynolds number of $\mathrm{Re} = 1.2 \times 10^{-4}$ with respect to the centreline velocity"[2]. The flow regime is considered *viscous* since $\mathrm{Re} << 1$. This regime is characterized by significant viscous effects such as internal friction and resistance to deformation which dominate over inertial forces.

The granular particles in the mixture are also subject to study using a non-dimensional number. The particle Reynolds number Re_p plays an important role for defining the momentum exchange between the fluid and granular phases. The definition of Re_p follows Equation [2.15] for which the the magnitude of the velocity of the fluid $\mathbf{u}_f$ is replaced by the magnitude of the slip velocity $||\mathbf{u}_f - \mathbf{u}_s||$ and the characteristic length l becomes the particle diameter d_p.

[2] From Monsorno et al. [2017]

2.2.2 Single phase flow

The purpose of this section is to introduce the single phase case in order to compare the results obtained with those of the flow of interest. the velocity profile of the fluid satisfies the following second-order ordinary differential equation (ODE) provided by Chin [2012]:

$$\frac{d^2 u_f(y)}{dy^2} = \frac{1}{\mu_f}\frac{dP}{dx} \tag{2.16}$$

The solutions to the ODE [2.16] are obtained by integrating it two times with respect to the variable y.

$$u_f(y) = \frac{1}{\mu_f}\frac{dP}{dx}\left(\frac{y^2}{2} + C_1 y + C_2\right) \quad \text{with } C_1, C_2 \in \mathbb{R} \tag{2.17}$$

The shear-rate of the flow follows an affine function given by Equation [2.18].

$$\dot{\gamma} = \frac{du_f(y)}{dy} = \frac{1}{\mu_f}\frac{dP}{dx}(y + C_1) \quad \text{with } C_1 \in \mathbb{R} \tag{2.18}$$

Equations [2.17] and [2.18] become unique only if adequate boundary conditions for the fluid velocity $u_f(y)$ are determined.
It is usually assumed that the *no-slip* condition is valid due to strong adhesive forces (see Section 2.4). This ensures the fluid sticks to the boundary, thus a zero velocity of the fluid at the wall is imposed. The velocity profile of a single phase fluid in a plane Poiseuille flow follows a quadratic law across the channel, the velocity attains its minimal values on both walls while its peak is in the centreline of the channel. The shear rate follows a linear law across the channel, its maximal values are on both boundary (i.e. $y = \pm\frac{l}{2}$) while its minimal value is at the centreline of the channel.

2.2.3 Two-phase flow

Let us now consider a granular suspensions in a plane Poiseuille flow under assumptions identical to the ones of the single-phase flow (i.e. constant fluid pressure gradient, constant fluid viscosity and small Reynolds number).

Several studies such as Xu et al. [2015], et al. [2018] and Chun et al. [2019] have already demonstrated that under the no-slip boundary condition for both phases, the velocity profile of the mixture follows a quadratic law similar to that obtained in the single phase case. Similarly, the shear rate follows a comparable behaviour with that of the single phase case, indeed it reaches its maximum at the walls and vanishes at the centreline of the channel. This observation is consistent with the particle migration induced by the flow as they moves towards a region of low shear rate.

The assumptions and conditions under which the previous studies were conducted are not quite the same to the ones in the present study. For instance et al. [2018] and Xu et al. [2015] do not completely neglect the effect of the gravity as the mixture is not considered *neutrally buoyant* (see Section 2.3). Chun et al. [2019] focuses on the bi-disperse suspensions under a plane Poiseuille flow, which means it considers a mixture containing two distinct groups of granular particles differing from one another on the size (large and small radius), unlike the present study which considers only granular spherical particles of the same radius.

2.3 Governing equations

The governing system of partial differential equations formed by Equations [2.9] and [2.14], defining the Navier-Stokes equations, is widely known to be difficult to solve. The difficulty is such that approximations and assumptions are required to make the system computationally tractable.
Let us summarize the different steps taken to get to the governing equations implemented in the numerical model.

2.3.1 Non-dimensionalisation

The governing equations used in the numerical simulation are expressed in non-dimensional form. "The non-dimensionalisation is performed with respect to the the fluid density $\hat{\rho}_r$, the fluid shear viscosity $\hat{\mu}_r$, the half-width of the channel $\hat{l}_r$ and the centreline velocity of the equivalent single-phase fluid flow $\hat{u}_r$"[3]. The aforementioned parameters are defined in the literature as follows :

$$\hat{\rho}_r = \rho_s \phi_s + \rho_f \phi_f \tag{2.19}$$

$$\hat{l}_r = l \tag{2.20}$$

$$\hat{\mu}_r = \frac{\rho_s \phi_s \mu_s + \rho_f \phi_f \mu_f}{\hat{\rho}_r} \tag{2.21}$$

$$\hat{u}_r = \frac{\rho_s \phi_s u_s + \rho_f \phi_f u_f}{\hat{\rho}_r} \tag{2.22}$$

2.3.2 Two-phase continuum model

Monsorno et al. [2016] provides an analytical study of the Navier-Stokes equations formed by Equations [2.9] and [2.14] and demonstrated that under a constant mass density of both phases (i.e. $\rho_k =$ constant for $k = \{f, s\}$), and, constant temperature for both phases and equal to one another (i.e. $T_f = T_s =$ constant), the Navier-Stokes equations reduces to the system of equations [2.23] - [2.27].
This system of differential equations consists of the balance of mass and momentum, while the balance of energy is omitted as it becomes trivial under the assumptions stated above.
Equation [2.27] is "called the compaction equation and describes the evolution of the volume fraction of the granular phase"[4].

Fluid phase

$$\frac{\mathrm{d}\phi_f}{\mathrm{d}_f t} = -\phi_f \nabla \cdot \mathbf{u}_f \tag{2.23}$$

$$\begin{aligned} \phi_f \frac{\mathrm{d}\mathbf{u}_f}{\mathrm{d}_f t} = &-\nabla \left(P_f \phi_f\right) + \frac{1}{\mathrm{Re}} \nabla \cdot \left(\left(\zeta_f \nabla \cdot \mathbf{u}_f\right) \phi_f \mathbf{I} + 2\phi_f \mathbf{V}_f^d \right) \\ &- \left(\delta \left(\mathbf{u}_f - \mathbf{u}_s\right) + P_f \nabla \phi_f\right) \end{aligned} \tag{2.24}$$

Granular phase

[3] From Monsorno et al. [2017]
[4] From Monsorno et al. [2016]

$$\frac{\mathrm{d}\phi_s}{\mathrm{d}_s t} = -\phi_s \nabla \cdot \mathbf{u}_s \tag{2.25}$$

$$\begin{aligned}\phi_f \frac{\mathrm{d}\mathbf{u}_s}{\mathrm{d}_s t} = &-\nabla\left(P_s \phi_s\right) + \frac{1}{\mathrm{Re}} \nabla \cdot \left(\left(\zeta_s \nabla \cdot \mathbf{u}_s\right) \phi_s \mathbf{I} + 2\mu_s \phi_s \mathbf{V}_s^d\right) \\ &+ \left(\delta\left(\mathbf{u}_f - \mathbf{u}_s\right) + P_f \nabla \phi_f\right) \\ &+ \frac{1}{\mathrm{Re}} \nabla \cdot \left(\mathcal{X}_a \phi_s \mathbf{I} + \mathcal{X}_b \phi_s \mathbf{V}_s \cdot \mathbf{V}_s\right) - \nabla \cdot \mathbf{C}_s\end{aligned} \tag{2.26}$$

Compaction equation

$$\frac{\mathrm{d}\phi_s}{\mathrm{d}_s t} = \frac{1}{\mathrm{Re}_c} \phi_s \phi_f \left(P_s - P_f - \beta_s + \nabla \cdot \left(\gamma_s \nabla \phi_s\right)\right) \tag{2.27}$$

The governing equations are composed of multiple parameters used as short-hand notations, these parameters are listed and defined below.
The material derivative with respect to the velocity $\mathbf{u}_k$ is defined as :

$$\frac{\mathrm{d}(\,\cdot\,)}{\mathrm{d}_k t} = \frac{\partial(\,\cdot\,)}{\partial t} + \mathbf{u}_k \cdot \nabla(\,\cdot\,) \qquad \forall\, k = \{s, f\} \tag{2.28}$$

The strain-rate tensor of phase k, $\mathbf{V}_k$, satisfies Equation [2.29] and has a different physical interpretation depending on the phase considered. For the granular phase, the strain-rate tensor $\mathbf{V}_s$ describes the relative deformation of the grains in space and time, whereas for the fluid phase, $\mathbf{V}_f$ characterizes how the velocity of the fluid changes in space and time within the fluid.

$$\mathbf{V}_k = \frac{\nabla \mathbf{u}_k + \nabla \mathbf{u}_k^T}{2} \qquad \forall\, k = \{s, f\} \tag{2.29}$$

The deviatoric part of $\mathbf{V}_k$, noted $\mathbf{V}_k^d$ is defined as :

$$\mathbf{V}_k^d = \mathbf{V}_k - \frac{1}{3} \mathrm{tr}\left(\mathbf{V}_k\right) \mathbf{I} \qquad \forall\, k = \{s, f\} \tag{2.30}$$

The interphasial momentum exchange f_k, introduced in the balance of momentum [2.14], is expressed in terms of the drag coefficient δ, the slip velocity $\mathbf{u}_f - \mathbf{u}_s$ and the pressure of the fluid phase. Since f_k describes the momentum exchange from a phase to another, the relationship between f_s and f_f must satisfy Newton's third law of motion and the principle of conservation of linear momentum. This condition translates to the vanishing sum of these terms, i.e. $f_s + f_f = 0$.

$$\begin{aligned} f_s &= -f_f \\ &= \delta\left(\mathbf{u}_f - \mathbf{u}_s\right) + P_f \nabla \phi_f \end{aligned} \tag{2.31}$$

The tensorial quantity $\mathbf{C}_s$ appearing in the balance of momentum of the granular phase [2.26] represents the Korteweg-type stresses. These stresses depend on the spatial distribution of the grains and are nonlocal in nature as they account for the finite size of the grains through the volume fraction of the granular phase.

$$\mathbf{C}_s = \gamma_s \nabla \phi_s \otimes \nabla \phi_s \tag{2.32}$$

The last short-hand notations are $\mathcal{X}_a$ and $\mathcal{X}_b$ and satisfy the following definition :

$$\mathcal{X}_a = -\sqrt{2}\mu_n \left(2\sqrt{\mathbf{V}_s^d : \mathbf{V}_s^d} - \frac{3}{2} \frac{\mathbf{V}_s^d : \mathbf{V}_s^d}{\sqrt{\mathbf{V}_s : \mathbf{V}_s}}\right) \tag{2.33}$$

$$\mathcal{X}_b = -\frac{\sqrt{2}\mu_n}{\sqrt{\mathbf{V}_s : \mathbf{V}_s}} \tag{2.34}$$

The governing equations are not exclusively composed of short-hand notations, there are more parameters to consider such as the transport coefficients (δ, μ_s and μ_n), the thermodynamic derivatives (β_s and γ_s). Let us define these parameters and list the relations employed in the current study.

The interphasial drag coefficient δ measures the friction and momentum transfer between the two phases. It is defined using the HKL-type correlation which makes the coefficient a function of the particle Reynolds number Re_p, the volume fraction of the granular phase ϕ_s and the particle diameter d_p.

$$\delta = f(\mathrm{Re}_p, \phi_s, d_p) \tag{2.35}$$

The shear viscosity coefficient μ_s measures the internal resistance of a fluid to shear deformation while the normal stress viscosity coefficient μ_n describes the capacity of a granular media to support normal viscous stresses resulting from shear deformation.

$$\mu_s = \frac{5}{2}\frac{1}{\phi_m - \phi_s} + \frac{1}{10}\frac{\phi_s}{(\phi_m - \phi_s)^2} \tag{2.36}$$

$$\mu_n = \frac{3}{4}\frac{\phi_s}{(\phi_m - \phi_s)^2} \tag{2.37}$$

Where ϕ_m is the critical value of the granular volume fraction at the jamming transition which is set to a value of 0.6.

The thermodynamic derivatives β_s and γ_s are determined empirically. Their constitutive relation should include a dependence on the microstructure of the granular phase (i.e. the volume fraction of the granular phase ϕ_s) as they relate to this microstructure. The intergranular stress β_s describes the resistance of solid particles to compaction, it is defined as :

$$\beta_s = \beta_0 \log\left(1 - \frac{\phi_s}{\phi_m}\right) \tag{2.38}$$

This formulation of β_s is consistent with its definition, in fact, β_s vanishes for small values of ϕ_s, and conversely it diverges as ϕ_s approaches ϕ_m.
The quantity γ_s is defined as the "derivative of the Helmholtz free energy of the granular phase with respect to $\nabla\phi_s$"[5].

$$\gamma_s = \gamma_0 \phi_s^6 \tag{2.39}$$

The coefficients γ_0 and β_0 are parameters that needs to be experimentally evaluated. The numerical model presented in Chapter 3 considers these parameters as inputs, their values will be set in Chapter 4.
The coefficient ζ_k represent the bulk viscosity of phase k, it measures the resistance of phase k to compression.

[5] From Monsorno et al. [2017]

2.3.3 Reduced governing equations

The two-phase continuum model described above does not consider the geometry of the problem at hand, it is therefore possible to reduce the complexity of the governing equations using additional constraints based on the geometry under consideration.

Monsorno et al. [2017] developed the reduced governing equations of the plane Poiseuille flow under the specific assumptions on the fluid flow and on the grains.
Let us seek time-independent solutions of the governing system of differential equations[2.23]-[2.27] that are unidirectional, which implies they follow the stream-wise direction and depend on the boundary-normal direction.
Let us assume that :

- The stream-wise direction follows the x-axis while the boundary-normal direction follows the y-axis.
- The flow is laminar as the Reynolds number is low and is set to $\mathrm{Re} = 1.2 \times 10^{-4}$.
- The half-channel width l is sufficiently small so that the mixture can be considered *neutrally buoyant*, its value is set to $l = 2.0 \times 10^{-5}$ mm. Consequently, the gravitational force is expected to be small enough to be neglected in the model.
- The velocity vectors are aligned in the stream-wise direction $\mathbf{1_x}$. Therefore :

$$\mathbf{u}_k = u_k(y)\mathbf{1_x} \qquad \forall\, k = \{s, f\} \tag{2.40}$$

  Where $\mathbf{1_x}$ is the unit vector in the direction of the x-axis.

- The granular volume fraction is dependent on the y-coordinate, and by extension so is the fluid volume fraction since the mixture is assumed to be saturated.

$$\phi_s = \phi_s(y) \tag{2.41}$$
$$\phi_f = 1 - \phi_s(y) \tag{2.42}$$

- In accordance with the above assumptions, the pressure of phase k, P_k, follows the stream-wise direction, i.e. $\mathbf{1}_x$, and depends on the y-coordinate. The pressure of phase k is then decomposed as :

$$P_k = p_k(y) - F_X \qquad \forall\, k = \{s, f\} \tag{2.43}$$

  Where F_X denotes the constant pressure gradient that drives the flow along the x-axis. Moreover, it has been proven that p_f is constant and, without loss of generality, is set to $p_f = 0$ for simplicity.

The system of differential equations [2.44] - [2.47] forms the reduced governing equations implemented in the numerical model studied.

Fluid phase

$$\frac{1}{\mathrm{Re}}\frac{d}{dy}\left((1-\phi_s)\frac{du_f}{dy}\right) = \delta\,(u_f - u_s) - F(1-\phi_s) \tag{2.44}$$

Granular phase

$$\frac{1}{\mathrm{Re}}\frac{d}{dy}\left(\mu_s\phi_s\frac{du_s}{dy}\right) = -\delta\left(u_f - u_s\right) - F\phi_s \tag{2.45}$$

$$\frac{1}{\mathrm{Re}}\frac{d}{dy}\left(\mu_n\phi_s\left|\frac{du_s}{dy}\right|\right) = -\frac{d}{dy}\left(\gamma_s\left(\frac{d\phi_s}{dy}\right)^2\right) - \frac{d}{dy}\left(p_s\phi_s\right) \tag{2.46}$$

Compaction equation

$$p_s - \beta_s + \frac{d}{dy}\left(\gamma_s\frac{d\phi_s}{dy}\right) = 0 \tag{2.47}$$

The reduced governing equations are composed of four differential equations, three balance of momentum equations for the granular phase and one for the fluid phase, and, the compaction equation which described the behaviour of the granular volume fraction. The reduced governing equations do not include the balance of mass as Equations [2.23] and [2.25] both become trivial under the assumptions introduced above.
This governing system of differential equations are composed of four differential equations and four variables, namely the granular volume fraction ϕ_s, the pressure of the granular phase p_s, and, the velocity of each phase u_f and u_s.

2.4 Boundary conditions

In order to solve the governing equations, boundary conditions are a requirement to that end. In a granular suspension, the granular and fluid phases require a priori different boundary conditions since each phase react differently with the boundary of the system. Indeed, a common assumption used for Newtonian fluid in a laminar flow is the *no-slip* boundary condition.

Definition 2.4.1 *The **no-velocity-offset** boundary condition, also known as the **no-slip** boundary condition states that the velocity of the fluid in direct contact with the boundary of the system equals the velocity of this boundary. This assumption translates to a zero tangential fluid velocity at the wall.*

Following the assumptions made in Section 2.3, the no-slip boundary conditions of the fluid is given by Equation [2.48].

$$u_f(y)|_{y=\pm1} = 0 \tag{2.48}$$

The physical interpretation of this boundary condition is that the adhesive forces between the fluid particles and the solid surface of the boundary of the system exceeds the cohesive forces existing between the fluid particles. The fluid then sticks to the wall of the system.
Note that the boundary points are located at $y = \pm1$ instead of $y = \pm l$ as presented in Section 2.2. This definition of the boundary points is the result of the non-dimensionalisation of the system.

The choice of the boundary condition for the granular phase is not as straightforward as it is for the fluid phase. Indeed, several studies have successfully modelled and reproduced the main characteristics of the flow under consideration with a no-slip boundary condition applied on the velocity of the granular phase (for instance Chun et al. [2019], Yeo and Maxey [2011], Monsorno et al. [2017]). However, these models do not accurately capture the behaviour of

the granular phase in the vicinity of the wall. Consequently, discrepancies remain between experimental data and numerical simulations regarding the volume fraction of the granular phase at the walls.
Recent studies suggest modifications regarding the choice of the boundary condition applied on the velocity of the granular phase. This proposition is supported by conclusive experimental evidence indicating the presence of a thin lubrication layer between the wall and the first layer of particles, where the shear rate is higher (Sochi [2011], Cloitre and Bonnecaze [2017],et al. [2022]). Therefore, experimental campaigns have explored increasing the surface roughness of the walls as a means of controlling the slip of the granular phase, suggesting that the no-slip boundary condition may not adequately describe the behaviour of the granular phase near the walls. According to Varsakelis et al. [2022], the most physically relevant alternative seems to be the *apparent slip* boundary condition.

Definition 2.4.2 *The **apparent slip** boundary condition is a Robin-type boundary condition whose form in the flow of interest is :*

$$u_s(y)|_{y=\pm 1} = \beta_w d_p \left(1 - \frac{\phi_s}{\phi_m}\right) \left(\frac{\mu_s}{\mu_f}\phi_s \left.\frac{du_s(y)}{dy}\right|_{y=\pm 1} + \phi_f \left.\frac{du_f(y)}{dy}\right|_{y=\pm 1}\right) \tag{2.49}$$

Where β_w denotes the slip coefficient which measures the slip between the grains and the surface of the boundary, and, d_p is the grain diameter.

The apparent slip boundary condition is sometimes described as a velocity discontinuity between the bulk flow and the surface wall. However, in accordance with Definition [2.4.2], the velocity at the wall remains continuous with that of the bulk flow.

For comparison purposes, let us first determine the effect of introducing slip on the boundary of the system using the *true-slip* boundary condition. The true-slip boundary conditions describes a situation in which the grains roll and slide along the wall of the system, the adhesive forces between the granular particles and the wall of the system are not sufficiently strong to reduce the tangential velocity to zero.

Definition 2.4.3 *The **true-slip** boundary condition states that the velocity of the granular phase in contact with the boundary of the system is proportional to a reference velocity.*

$$u_s(y)|_{y=\pm 1} = A_{slip}\, u_{max} \tag{2.50}$$

Where A_{slip} is the slip coefficient whose values lies in the interval $0 < A_{slip} \leq 1$.

In the literature, the choice of the reference velocity in Equation [2.50] is the maximal velocity of the mixture, which lays at the centre of the channel.

The boundary condition associated to the granular volume fraction ϕ_s is given below.

$$\int_{-1}^{1} \phi_s(y)dy = 2\overline{\phi}_s \quad \text{and} \quad \phi_s(y)|_{y=-1} = \phi_s(y)|_{y=1} \tag{2.51}$$

This condition accounts for the one-dimensional nature and symmetry of the flow, while assuming the average granular volume fraction $\overline{\phi}_s$ to be a known quantity.

This boundary condition ensures the conservation of the granular volume fraction in the channel and is therefore referred to as a conservation-type boundary condition.

The Last boundary condition to define is for the granular pressure p_s. It is defined using a Dirichlet boundary condition via the following equation.

$$p_s(y)|_{y=1} = \beta_s \left(\phi_s(y)|_{y=1}\right) \tag{2.52}$$

This condition exploits the symmetry of the system to apply Equation [2.52] on both walls.This symmetry property results from the boundary condition imposed on the granular volume fraction ϕ_s and the fact that the intergranular stress β_s is a function of the granular volume fraction.

3 Numerical methodology

3.1 Simulation setup

The simulations were performed by varying different parameters individually to facilitate comparison between the different cases.
In this study, the term *physical parameters* refers to the inputs of the numerical model that govern its physical behaviour, whereas *solver parameters* refers to the inputs that determine how the computer solves the reduced governing equations.
The physical parameters considered for variations are listed below.

- The average volume fraction of the granular phase $\overline{\phi}_s$: 0.298 and 0.411
- The constant pressure gradient F_X: 95000.0 and 169560.0
- The thermodynamic coefficient γ_0: 0.5, 0.05, 0.005 and 0.0005
- The intergranular stress coefficient β_0: 10^{-8}, 10^{-9} and 10^{-10}
- The boundary condition applied on the velocity of the granular phase: no-slip, true-slip and apparent-slip.

Note that the values of ϕ_s and F_X are linked. Indeed, an increase in the amount of grains in the mixture corresponds to an increase of $\overline{\phi}_s$ which in turn increases the shear resistance of the mixture. Therefore a greater driving force is required to maintain a similar flow, which translates to a greater value of the constant pressure gradient F_X. In conclusion, modifying the average volume fraction of the granular phase $\overline{\phi}_s$ requires to adjust the constant pressure gradient F_X in accordance. The average volume fraction set at 0.298 and 0.411 corresponds respectively to a value of the constant pressure gradient F_X of 95000 and 169560.
It should be noted that $\beta_0 = 0.05$ and $\gamma_0 = 10^{-9}$ are used as baseline values for comparison purposes. Accordingly, when β_0 is modified, γ_0 is kept fixed at 10^{-9} and vice-versa.

Aside from the physics parameters presented above, the solver parameters were modified only to reduce or increase the rate of convergence and reduce the CPU strain. These parameters are the following.

- The maximal number of iterations.
- The number of points to discretize the 1-D grid.
- The tolerance ϵ on the l_2-norm, which defines the convergence criterion.

- The under-relaxed factor, which defines the convergence rate and the stability of the simulation.

A third category of parameters referred to as the *reference parameters* is introduced. These parameters consist of the input values used to transform each parameter and variable into its non-dimensional form. The relations presented in Section 2.3.1 can not be applied in the present study since some of the required values are variables to be determined at the end of the simulation, namely u_k and ϕ_k with $k = \{s, f\}$. The reference parameters are listed below.

- The shear viscosity of reference : $\hat{\mu}_r = 0.04$ [kg / (m.s)]
- The density of reference : $\hat{\rho}_r = 1200$ [kg / m^3]
- The half-channel width : $\hat{l}_r = 2 \times 10^{-5}$ [m]
- The velocity of reference : $\hat{u}_r = 0.0002$ [m / s^2]

These reference values satisfies the assumption made in Section 2.3.3 regarding the value of the Reynolds number Re.
As the relations presented in Section 2.3.1 are not used, the non-dimensionalisation of the outputs of the numerical model satisfies the following.

$$u_k^{\text{out}} = \frac{u_k}{\hat{u}_r} \qquad \forall k = \{s, f\} \tag{3.1}$$

$$p_s^{\text{out}} = \frac{p_s}{\hat{\rho}_r \left(\hat{u}_r\right)^2} \tag{3.2}$$

The granular volume fraction ϕ_s is by definition non-dimensional and therefore requires no modifications.

3.2 Numerical algorithm

The numerical algorithm used to solve the governing equations [2.44] - [2.47] is the segregated Picard-iteration algorithm, and a second-order centred differences scheme is used to compute the derivatives.
The segregated Picard iteration algorithm decouples the governing system of equations into a set of independent equations that are solved sequentially. This is an iterative method, thus the solutions progressively become more accurate with each iteration.

3.2.1 Discretization

The governing equations are discretized using the centred difference scheme which stipulates that the first- and second-order derivatives can be approximated using finite differences. Let ψ be a twice continuously differentiable function, its first- and second order derivatives are evaluated as follows :

$$\frac{d}{dy}\psi(y) \approx \frac{\psi(y + \Delta y) - \psi(y - \Delta y)}{2\Delta y} = \tag{3.3}$$

$$\frac{d^2}{dy^2}\psi(y) \approx \frac{\psi(y + \Delta y) - 2\psi(y) + \psi(y - \Delta y)}{(\Delta y)^2} \tag{3.4}$$

To keep track of the iterations at which the computations are performed and the position within the grid at which it was computed, the superscript n is introduced to represent the iteration number while the subscript i denotes the corresponding grid point. Therefore, Equations [3.3] and [3.4] can be written at iteration n as follows :

$$\left.\frac{d}{dy}\psi(y)\right|_{y=i} \approx \frac{\psi_{i+1}^n - \psi_{i-1}^n}{2\Delta y} \tag{3.5}$$

$$\left.\frac{d^2}{d^2y}\psi(y)\right|_{y=i} \approx \frac{\psi_{i+1}^n - 2\psi_i^n + \psi_{i-1}^n}{(\Delta y)^2} \tag{3.6}$$

Where Δy represents the discretization step between consecutive points along the y-axis.

3.2.2 Under-relaxation factor

The under-relaxation factor is introduced to improve the stability of the iterative solutions obtained by the algorithm. This factor limits the changes a variable undergoes between two successive iteration. It is necessary to control the changes of the variables due to the non-linearity nature of the governing equations. The under-relaxation is implemented using the following update-rule.

$$\psi_i^{n+1} = (1-\lambda)\,\psi_i^n + \lambda\psi_i^\star \tag{3.7}$$

Where λ is the relaxation factor whose values are in the interval $0 \leq \lambda \leq 1$, and, $\psi_i^\star$ refers to the intermediate value obtained by solving a discretized equation.
Note that if $\lambda = 0$, there are no updates and each iteration remains identical to the previous one. Conversely, if $\lambda = 1$ the next iteration is equal to the intermediate value obtained by solving the semi-implicit scheme, which means that the intermediate value is fully accepted without under-relaxation.
There exist a trade-off between the convergence rate and the numerical stability of the algorithm. Indeed, as the value of λ decreases, the convergence rate decreases as well while the numerical stability improves.

3.2.3 Initial conditions

The initial conditions refers to the starting values of the unknowns of the system. These values are set to the following values :

$$u_{s_i}^0 = 0, \qquad u_{f_i}^0 = 0, \qquad \phi_{s_i}^0 = \overline{\phi}_s, \qquad p_{s_i}^0 = \beta_s\left(\overline{\phi}_s\right) \tag{3.8}$$

These initial values are valid at the first iteration $n = 0$ for all points in the grid.

3.2.4 Computation sequence

The program starts with first-guess values for the unknown p_s, u_f, u_s and ϕ_s as given in Equation [3.8]. The program then proceeds with solving the discretized governing equations. The equations are solved sequentially, following the order in which the intermediate values are obtained: $\phi_s^\star$, $u_f^\star$, $u_s^\star$ and finally $p_s^\star$.

The intermediate value $\phi_s^\star$ is obtained by solving the semi-implicit scheme of the compaction equation [2.47].

$$\left(\gamma_{s_i}^n + \gamma_{s_{i+1}}^n\right)\phi_{s_{i+1}}^\star - \left(\gamma_{s_{i-1}}^n + 2\gamma_{s_i}^n + \gamma_{s_{i+1}}^n\right)\phi_{s_i}^\star + \left(\gamma_{s_{i-1}}^n + \gamma_{s_i}^n\right)\phi_{s_{i-1}}^\star = -2\left(\Delta y\right)^2\left(p_{s_i}^n - \beta_{s_i}^n\right) \tag{3.9}$$

The intermediate value of $u_f^\star$ is determined by solving the semi-implicit scheme of the balance of momentum of the fluid phase [2.44].

$$-\left(\phi_{s_i}^n + \phi_{s_{i+1}}^n\right)u_{f_{i+1}}^\star + \left(\phi_{s_{i-1}}^n + 2\phi_{s_i}^n + \phi_{s_{i+1}}^n\right)u_{f_i}^\star - \left(\phi_{s_{i-1}}^n + \phi_{s_i}^n\right)u_{f_{i-1}}^\star = 2\,\mathrm{Re}\left(\Delta y\right)^2\left[\delta_i^n\left(u_{f_i}^n - u_{s_i}^n\right) - F\left(1-\phi_{s_i}^n\right)\right] \tag{3.10}$$

The intermediate value of $u_s^\star$ is computed the same way the previous values were, by solving the semi-implicit scheme of Equation [2.45].

$$\left(\mu_{s_i}^n\phi_{s_i}^n + \mu_{s_{i+1}}^n\phi_{s_{i+1}}^n\right)u_{s_{i+1}}^\star - \left(\mu_{s_{i-1}}^n\phi_{s_{i-1}}^n + 2\mu_{s_i}^n\phi_{s_i}^n + \mu_{s_{i+1}}^n\phi_{s_{i+1}}^n\right)u_{s_i}^\star + \left(\mu_{s_{i-1}}^n\phi_{s_{i-1}}^n + \mu_{s_i}^n\phi_{s_i}^n\right)u_{s_{i-1}}^\star = -2\,\mathrm{Re}\left(\Delta y\right)^2\left[\delta_i^n\left(u_{f_i}^n - u_{s_i}^n\right) - F\phi_{s_i}^n\right] \tag{3.11}$$

The last intermediate value to be computed is $p_s^\star$, which is determined using Equation [2.46]. This differential equation is integrated yielding the following result :

$$-\frac{1}{\mathrm{Re}}\mu_n\phi_s\left|\frac{du_s}{dy}\right| - \gamma_s\left(\frac{d\phi_s}{dy}\right)^2 + C = p_s\phi_s \tag{3.12}$$

Where C is the integration constant.
The discretization of [3.12] yields the following semi-implicit scheme :

$$-\frac{1}{\mathrm{Re}}\mu_{n_i}^n\phi_{s_i}^n\frac{\left|u_{s_{i+1}}^n - u_{s_{i-1}}^n\right|}{2\Delta y} - \gamma_{s_i}^n\frac{\left(\phi_{s_{i+1}}^n - \phi_{s_{i-1}}^n\right)^2}{4\left(\Delta y\right)^2} + C = p_{s_i}^\star\phi_{s_i}^\star \tag{3.13}$$

The expression of the integration constant C is not given as it is long and cumbersome, however it should be noted that C is a function of β_s, the Reynolds number Re, the slip velocity $||\mathbf{u_f} - \mathbf{u_s}||$, the volume fraction of the granular phase ϕ_s, γ_s and μ_n.

Once all intermediate values have been computed, the relative error ϵ is evaluated using the l_2-norm to determine whether the convergence criterion is satisfied. Convergence is attained if the relative errors associated with all four unknowns (i.e. ϕ_s, u_f, u_s and p_s) are all below the threshold value set for the convergence.

$$\epsilon = \frac{||\psi_i^\star - \psi_i^n||_2}{\psi_i^n} \qquad \forall i \in [0, N-1] \tag{3.14}$$

If the convergence criterion is not met, all unknowns are updated for the next iteration $n+1$ using Equation [3.7].

Note that all the computations above assume that $i \in [1, N-2]$ where N denotes the number of points in the grid. The boundary points $i = 0$ and $i = N-1$ are accounted for using the boundary conditions, which are implemented according to the procedure described in Section 3.3.

3.3 Boundary Conditions

The numerical algorithm is not complete without the boundary conditions introduced in Section 2.4. The complexity of implementing a boundary condition depends on its type. There are three types of boundary conditions considered in this project: Dirichlet boundary conditions, Robin-type boundary condition and finally a conservation-type boundary condition.
The boundary condition applied on each unknown is computed simultaneously with the unknowns of the bulk that need to be determined at the corresponding step of the resolution sequence. Therefore, the intermediate values on the walls of the channel are first determined before being updated using Equation [3.7].

The boundary condition applied to the granular volume fraction ϕ_s is a conservation-type boundary condition. This implies that all the variables, those of the bulk and those on the walls of the channel, need to be considered in the numerical formulation. The definite integral present in Equation [2.51] is translated to a finite summation in the numerical model.

$$\sum_{i=0}^{N-1} \phi^\star_{s_i} = 2\overline{\phi}_s \quad \text{and} \quad \phi^\star_{s_0} = \phi^\star_{s_{N-1}} \tag{3.15}$$

The constraint applied to the fluid velocity on the surface walls is the no-slip boundary condition. This constraint follows Equation [2.48], which is easily implemented as it is a Dirichlet boundary condition.

$$u^\star_{k_i} = 0 \tag{3.16}$$

This formulation of the fluid velocity is valid only on the walls, implying that $i = 0$ and $i = N - 1$.

The constraint applied to the granular velocity depends on the choice made before the execution of the program. If the no-slip boundary condition is selected, then it follows the expression [3.16] with the sole difference that $u^\star_{f_i}$ is replaced by $u^\star_{s_i}$.

The *true-slip* boundary condition described in Definition [2.4.3] is implemented as follows.

$$u^\star_{s_i} = A_{slip} u^\star_{s_m} \tag{3.17}$$

Where $m = (N-1)/2$ denotes the middle point of the y-axis grid at which the maximal velocity $u^\star_{s_m}$ is predicted to occur.

The apparent-slip constraint is a Robin-type boundary condition, which requires the discretization of the derivative present in Equation [2.49]. Note that using a central finite difference on the boundary is not recommended on a boundary as it would require the use of a ghost point which would increase the size of the grid. The method employed was to consider the symmetry of the channel and to use a forward finite difference on the wall.
The first-order forward finite difference evaluates first-order derivative as follows.

$$\left.\frac{d}{dy}\psi(y)\right|_i \approx \frac{\psi^n_{i+1} - \psi^n_i}{\Delta y} \tag{3.18}$$

The apparent-slip boundary condition is implemented and given by the expression below.

$$u^{\star}_{s_i} = \beta_w d_p \left(1 - \frac{\phi^n_{s_i}}{\phi_m}\right) \left(\frac{\mu^n_{s_i}}{\mu_f} \frac{u^{\star}_{s_{i+1}} - u^{\star}_{s_i}}{\Delta y} + \left(1 - \phi^n_{s_i}\right) \frac{u^n_{f_{i+1}} - u^n_{f_i}}{\Delta y}\right) \tag{3.19}$$

Note that the coefficient β_w is set to unity, and μ_f denotes the fluid viscosity coefficient. Since Equation [3.19] uses a forward-finite difference scheme, the subscript i is set to 0. The symmetry of the channel allows $u_{s^{\star}_{N-1}}$ to be equal to $u_{s^{\star}_0}$.

The last constraint to implement is a Dirichlet boundary condition applied to the granular pressure p_s. Its formulation is given below.

$$p^{\star}_{s_i} = \beta_0 \log\left(1 - \frac{\phi^{\star}_{s_i}}{\phi_m}\right) \tag{3.20}$$

4 Numerical results and discussion

The simulations were performed to compare the different boundary conditions applied to the velocity of the granular phase. Accordingly, the simulations are divided into three main groups: *no-slip*, *true-slip*, and *apparent-slip*.
Within each group, the simulations are further divided into two subgroups according to the average volume fraction of the granular phase $\overline{\phi}_s$ and, consequently, the corresponding constant pressure gradient driving the flow F_X.
Finally, within each subgroup, the simulations are divided into two categories: variations of γ_0 while keeping β_0 constant, and vice versa. This results in six simulations per subgroup.

This chapter is structured into three sections. The first three present the results concerning the granular volume fraction ϕ_s, the granular pressure p_s, and the velocity u_f and u_s.

The algorithm was validated under the *no-slip* boundary conditions applied on the granular velocity u_s by the Louvain School of Engineering in the paper Monsorno et al. [2017]. Consequently, the results obtained under this boundary condition will serve as a point of comparison for the *true-* and *apparent-* slip boundary conditions.

4.1 Volume fraction

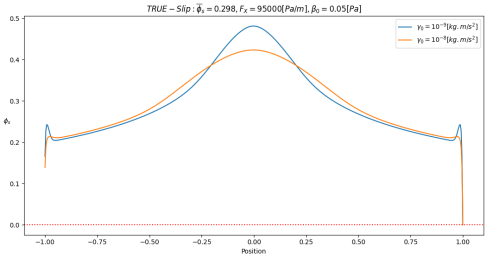

(a) True-slip

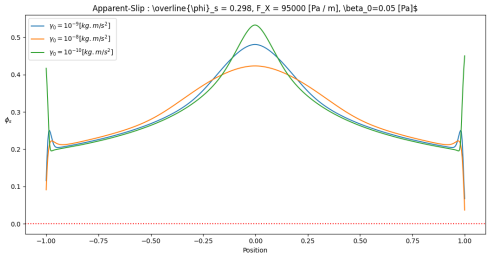

(b) Apparent-slip

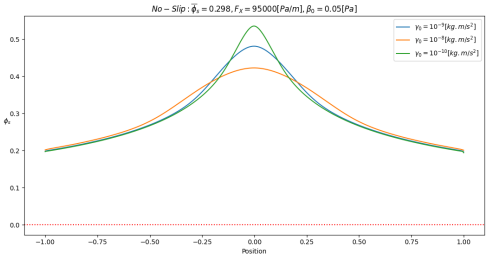

(c) No-slip

Figure 4.1: Granular volume fraction for $\beta_0 = 0.05[\text{Pa}]$ and $\overline{\phi}_s = 0.298$

The first observation is that the true-slip and apparent-slip cases exhibit profiles similar to those obtained for the no-slip case. The main expected difference between the three configurations lies in the behaviour of the granular volume fraction at the walls. In both slip cases, granular particles are present at the surface walls of the channel. Interestingly, the results obtained for $\gamma_0 = 10^{-8}$ and $\gamma_0 = 10^{-9}$ are nearly identical. Note that there is no result of the true-slip case for $\gamma_0 = 10^{-10}$ due to many errors occurring and preventing any form of correct data to be exploited. These errors range from a poorly chosen under-relaxation factor to false convergence, i.e. the program assumes convergence as there the relative difference is respected but there are no physical meaning behind these kind of results.
The granular particle concentration for $\gamma_0 = 10^{10}$ in the apparent-slip case exhibits a peculiar behaviour near the boundary of the channel. Indeed ϕ_s increases drastically at these locations compared to the other values of γ_0. This result may indicate an extreme case of reduced shear rate, or this corresponds to an edge case, i.e. an input parameter that approaches the limit of the numerical model. This behaviour can only be determined by examining the other results obtained under the same conditions. Before doing so, let us determine the effects of γ_0 on the granular volume fraction ϕ_s.
The influence of γ_0 is shown in Figure [4.1], as γ_0 decreases the concentration of grains increases in the centreline of the channel. This phenomenon can be explained by combining the compaction equation [2.47] with the definition of γ_s given by Equation [2.39]. The resulting expression makes the influence of the coefficient γ_0 on ϕ_s explicit.

$$p_s - \beta_s + \gamma_0 \frac{d}{dy}\left(\phi_s^6 \frac{d\phi_s}{dy}\right) = 0 \tag{4.1}$$

The algorithm solves the compaction equation by treating p_s and β_s as parameters whose values are set to those obtained in the previous iteration while considering ϕ_s as the variable of the equation. Consequently, the granular volume fraction profile is inversely proportional to the value of γ_0 which corroborates the observation made. Indeed, the resolution of the first step of the algorithm (at iteration n) consists of solving a tridiagonal matrix whose solutions are proportional to the constant vector.

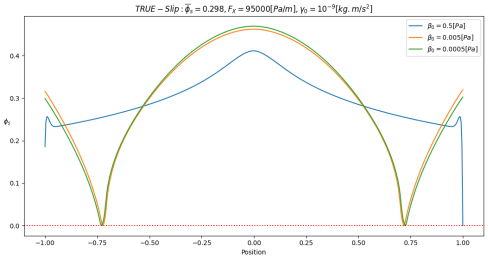

(a) True-slip

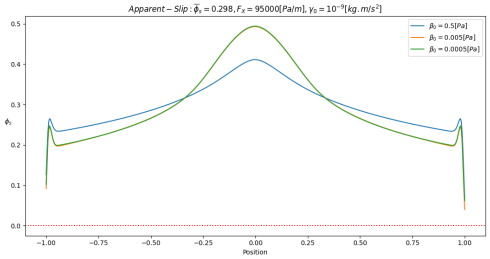

(b) Apparent-slip

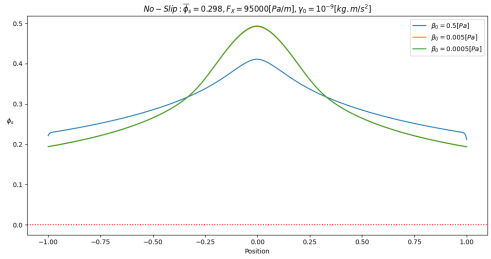

(c) No-slip

Figure 4.2: Granular volume fraction for $\gamma_0 = 10^{-9}[kg\,m/s^2]$ and $\overline{\phi}_s = 0.298$

Figure [4.2] presents the granular volume fraction profiles obtained while keeping γ_0 constant. Let us determine how the variations of β_0 has an effect on the granular volume fraction. Comparing the apparent-slip and the no-slip cases reveals similar behaviour. As expected, the main difference lies in the behaviour on the surface walls. A complementary observation is that decreasing the value of β_0 leads to an increase of the concentration of granular particles in the centreline of the channel. This is explained by recalling that $\beta_s(\phi_s)$ is defined as the intergranular stress, which characterizes the resistance of the granular phase to compaction. Therefore, a lower value of β_0 corresponds to a lower resistance to compaction, allowing more particles to migrate towards the centreline.
For the true-slip case, it should be noted that for $\beta_0 = 0.5$, the granular volume fraction profile is nearly identical to those of the apparent- and no-slip cases. However, for β_0 set to 0.005 and 0.0005 the profile reaches a zero-value around the points $y \approx \pm 0.7$. This abrupt change in behaviour between 0.05 and 0.005 and the vanishing granular volume fraction seems to deviate from the expected physical behaviour of a granular suspension under plane Poiseuille flow. This suggests that true-slip boundary condition reached an edge case. The lower limit of β_0 in the true-slip case is, a priori, 0.005.

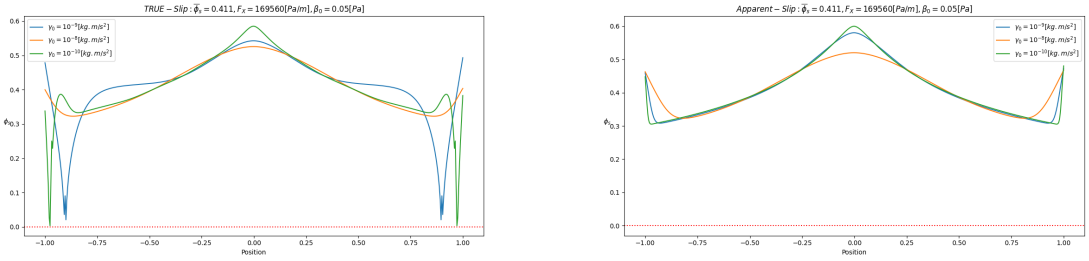

(a) True-slip (b) Apparent-slip

Figure 4.3: Granular volume fraction for $\beta_0 = 0.05[\text{Pa}]$ and $\overline{\phi}_s = 0.411$

Let us examine the influence the average granular volume fraction grain size $\overline{\phi}_s$, and by extension the constant pressure gradient F_X, has on the previous results.
An obvious but nonetheless important observation is that increasing the average volume fraction directly shifts each granular volume fraction profile upwards. Note that the no-slip case is not included, as it does not exhibit any significant differences from the profiles presented previously, unlike the true- and apparent-slip cases. Aside from the overall profile shape, the main noticeable difference is the behaviour of the granular volume fraction on the surface walls of the channel in the true- and apparent-slip cases.

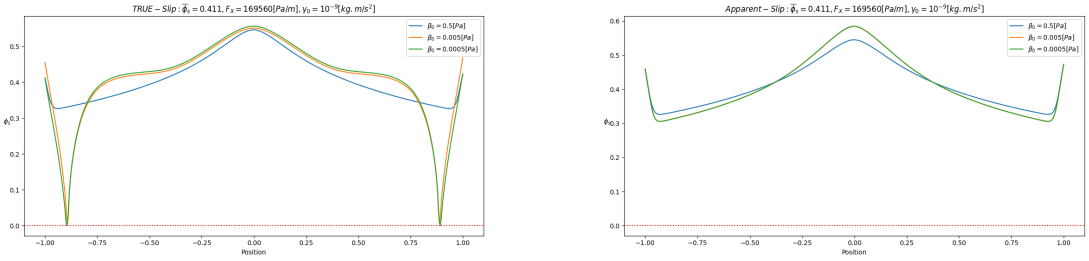

(a) True-slip (b) Apparent-slip

Figure 4.4: Granular volume fraction for $\gamma s = 10^{-9}[kg\,m/s^2$ and $\overline{\phi}_s = 0.411$

Let us first review the results obtained in the true-slip case, Figures [4.3a] and [4.4a] show that the vanishing granular volume fraction observed previously reappears, although it is now located closer to the surface walls of the channel. The edge-case seems to occur for similar values of β_0. However when β_0 is kept constant, values of γ_0 that were previously physically correct no longer do. It seems that increasing the average volume fraction have reduced the tolerance of the program against edge-case associated with γ_0 parameter.

4.2 Pressure

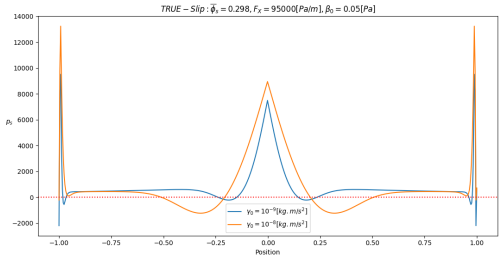

(a) True-slip

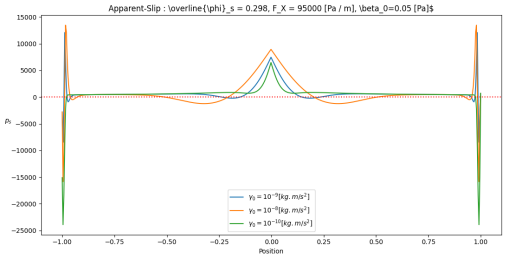

(b) Apparent-slip

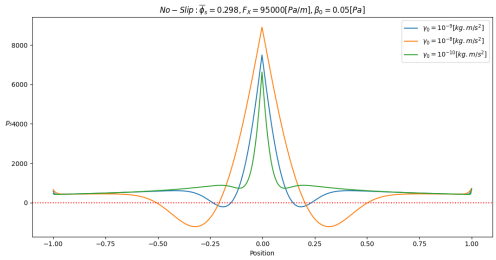

(c) No-slip

Figure 4.5: Granular pressure for $\beta_0 = 0.05[\text{Pa}]$ and $\overline{\phi}_s = 0.298$

Figure [4.5] shows the granular pressure p_s across the boundary conditions and the variation of γ_0. Note that the sign of the granular pressure has a physical meaning. A positive pressure denotes a compressive stress acting on the granular particles whereas a negative pressure corresponds to a tensile stress. These two types of stress respectively result in the compaction and expansion of the granular phase, with the latter causing the grains to move away from one another.
All the granular pressure profiles exhibit the same behaviour. As the value of γ_0 decreases, the peak pressure of the compaction zone in the middle of the channel decreases whereas the width of the compaction zone becomes narrower. It is observed that at $\gamma_0 = 10^{-10}$, the granular pressure is a priori positive everywhere in the channel except on the boundaries. The effect of the narrower compaction zone can also be observed in the granular volume fraction profile. Indeed, when reviewing each granular pressure profile with its associated granular volume fraction profile, it can be observed that the concentration of granular particles in the centreline of the channel is directly correlated to the granular pressure distribution.

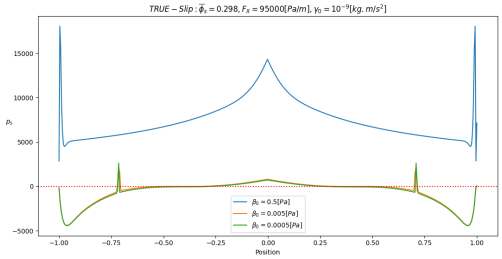

(a) True-slip

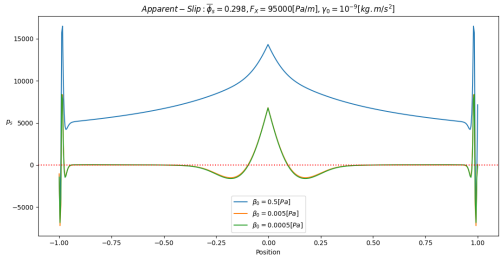

(b) Apparent-slip

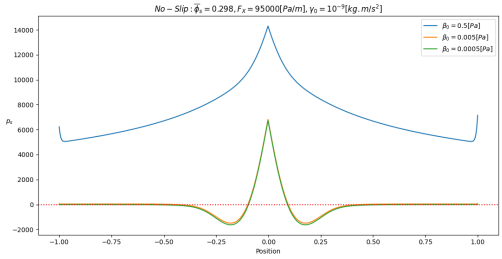

(c) No-slip

Figure 4.6: Granular pressure for $\gamma_s = 10^{-9}[kg\,m/s^2]$ and $\overline{\phi}_s = 0.298$

Following the observations made earlier concerning the link between the granular volume fraction and the granular pressure, which already existed in the governing equations, it is only natural to extend the verification with the variations of β_0.
The values for which there was an edge-case are consistent with the observations made in Section 4.1. The effect of these edge-cases manifests as a spike at the location where the granular volume fraction vanishes.

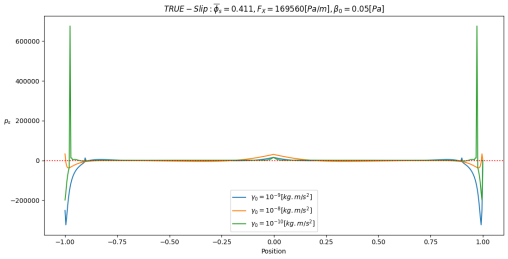

(a) True-slip

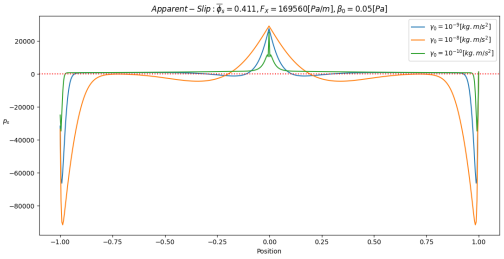

(b) Apparent-slip

Figure 4.7: Granular volume fraction for $\beta_0 = 0.05[\text{Pa}]$ and $\overline{\phi}_s = 0.411$

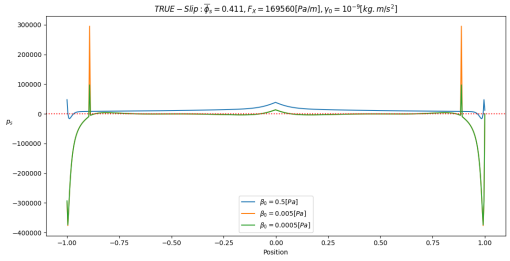

(a) True-slip

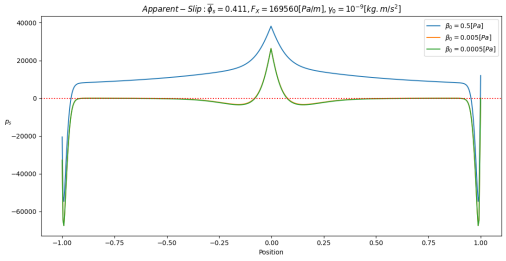

(b) Apparent-slip

Figure 4.8: Granular volume fraction for $\gamma s = 10^{-9}[kg\,m/s^2$ and $\overline{\phi}_s = 0.411$

Figures [4.7a] and [4.8a] shows the effects of an edge-case applied on the pressure profile. The values around the boundary of the channel takes values that have no physical meaning to it.

4.3 Velocity

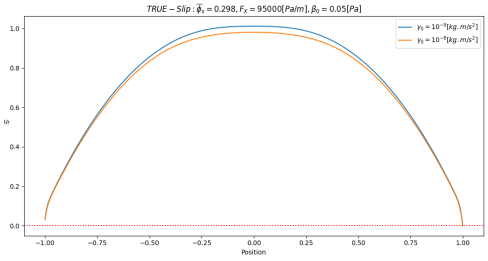

(a) True-slip

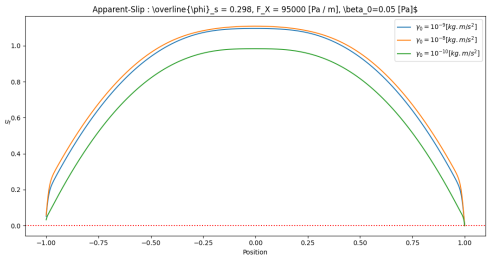

(b) Apparent-slip

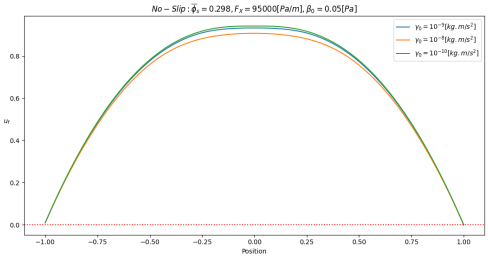

(c) No-slip

Figure 4.9: Fluid velocity for $\beta_0 = 0.05$[Pa] and $\overline{\phi}_s = 0.298$

Figure [4.10] presents the fluid velocity profiles obtained while keeping β_0 constant. The first observation is that the influence of γ_0 on the fluid velocity differs between the apparent-slip case, and the no- and true-slip cases. In the apparent-slip case, the maximum fluid velocity decreases as γ_0 decreases. Conversely, for the no- and true-slip cases, the maximum fluid velocity increases as γ_0 decreases.
The second observation is that the fluid velocity profile for the apparent-slip case exceeds

unity, indicating that the fluid velocity surpasses the reference value. In contrast, the maximum velocities for the no- and true-slip cases remain respectively around 0.8 and 1. This can be explained by the differences in the behaviour of the granular particles near the surface walls. Indeed, for a granular particle to move faster it must to encounter less resistance of flow, i.e. the lesser the shear stress, the faster the granular particles move. Each boundary conditions applied on the granular phase has a different shear rate profile at the boundary of the channel. The no-slip boundary conditions has the highest shear rate of the three since the tangential velocity is always set to zero. The true-slip constraint sees its shear rate be less than of the no-slip, and finally the apparent-slip condition is assumed to have an even lower shear rate. The link between the shear rate and shear stress is the following.

$$\text{shear stress} = \mu_f \, \text{shear rate} \tag{4.2}$$

Where μ_f is the fluid viscosity and constant across all simulations. The apparent-slip case possesses the lowest shear rate, so the lowest shear stress and in turn has the fastest velocity profile.

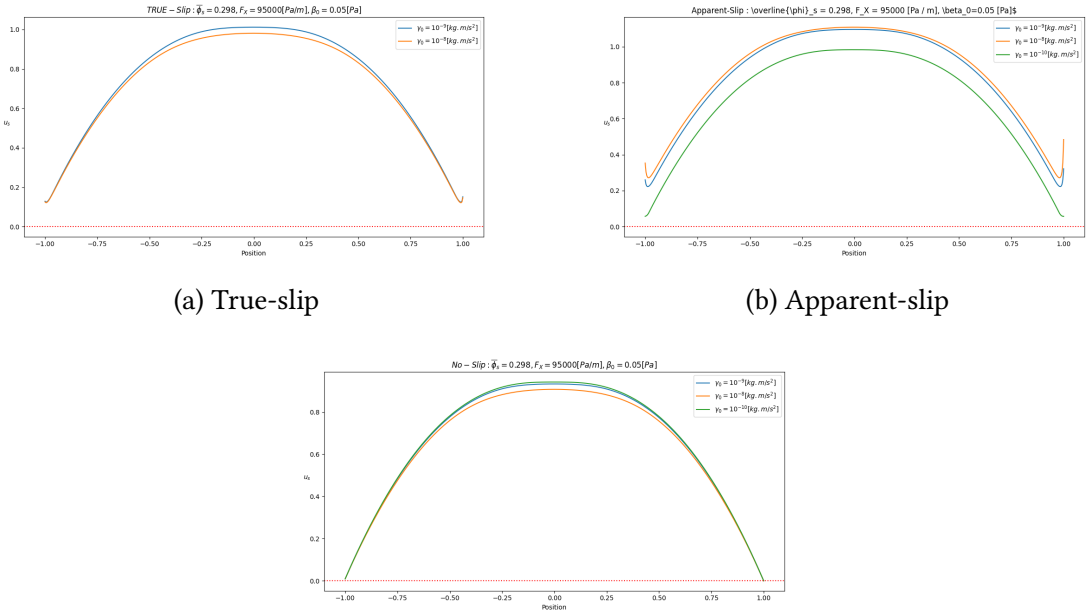

(a) True-slip

(b) Apparent-slip

(c) No-slip

Figure 4.10: Granular velocity for $\gamma_0 = 10^{-9}[kg\,m/s^2]$ and $\overline{\phi}_s = 0.298$

Let us consider the granular velocity profiles and compare them with the corresponding fluid velocity profiles. The comparison shows that the velocity of the granular phase u_s and that of the fluid phase u_f are nearly identical, with the latter being slightly faster. This can be explained by a strong viscous drag that exchanges momentum between the two phases. Indeed, by using the expression of the semi-implicit scheme [3.10] and considering that the drag coefficient δ_i^n is a relative large number, it follows that the velocity slip $u_{f_i}^n - u_{s_i}^n$ must remain small in comparison for the right-hand side of the scheme to remain a finite number.

5 Conclusion

The objective of this master thesis was to investigate the influence of the boundary condition applied to the solid phase of a dense granular suspension under a laminar plane Poiseuille flow. This work accounted for three constraints that were compared between each other, namely the *no-slip*, the *true-slip* and the *apparent-slip* boundary conditions.

The numerical study was conducted using a two-phase continuum model describing the fluid and granular phases. This system of equations was complicated to implement, therefore a reduced governing system of equations was determined using the geometry of interest. The numerical algorithm used in this study was provided and developed within the Louvain School of Engineering. This algorithm implements the reduced governing equations and are solved after discretization of its unknown.

The profiles of each output shows that the boundary condition applied on the granular velocity has a limited influence en the shape of its curve. Varying the coefficients γ_0 and β_0 shows the limit of the program when the *true-slip* constraint is considered.
The *true-slip* boundary conditions, despite its simple expression, has the most difficulties to reach convergence. There are three main reasons for such a low convergence rate. Firstly, the simulation might run into a singular matrix due to a vanishing ϕ_s, this observation is especially true if a simulation involves the *true-slip* boundary condition.
Secondly, the small under-relaxation factor needed to maintain stability which can make a simulation run for over a month before converging. Finally, the simulation might wrongly converge to a solution that has no physical meaning to it.

The simulations done in this master thesis proved the limit of the algorithm for certain values of the studied parameters as some were edge-case for the *true-slip* constraint.
Further simulations should be considered, with more varying values of γ_0 and β_0, to determine if the range of physically plausible solutions is restricted. The numerical algorithm could improve its robustness against instability associated to the *true-slip* constraint. The boundary conditions, especially the *apparent-slip* constraint, could be updated as there are more studies on the subject nowadays.

Bibliography

B. Andreotti, Y. Forterre, and O. Pouliquen. Granular Media: Between Fluid and Solid. Cambridge University Press, Cambridge, 2013.

Nicolas Borghini. Elements of hydrodynamics. Universität Bielefeld, Fakultät für Physik, September 2015. URL https://fr.scribd.com/document/635734760/Untitled.

Wilson C. Chin. More steady flow applications. In Managed Pressure Drilling, pages 183–266. Gulf Professional Publishing, 2012.

B. Chun, J.S. Park, H.W. Jung, and Y.Y. Won. Shear-induced particle migration and segregation in non-brownian bidisperse suspensions under planar poiseuille flow. Journal of Rheology, 63(3):437–453, 2019.

Michel Cloitre and Roger T. Bonnecaze. A review on wall slip in high solid dispersions. Rheologica Acta, 56(3):283–305, March 2017.

Adam Djellouli. Central difference method, March 2026. URL https://adamdjellouli.com/articles/numerical_methods/3_differentiation/central_difference.

Donald A. Drew and Stephen L. Passman. Theory of Multicomponent Fluids. Springer-Verlag, New York, 1999.

I. Kwon et al. Particle migration in planar couette-poiseuille flows of concentrated suspensions. Journal of Rheology, 62(2):419–435, 2018.

M. Saldana et al. The reynolds number: A journey from its origin to modern applications. Fluids, 9(12):299, 2024.

P. Wilms et al. On the difficulty of determining the apparent wall slip of highly concentrated suspensions in pressure driven flows: The accuracy of indirect methods and best practice. Journal of Non-Newtonian Fluid Mechanics, 299:104694, January 2022.

S. Gallier, E. Lemaire, F. Peters, and L. Lobry. Rheology of sheared suspensions of rough frictional particles. Journal of Fluid Mechanics, 757:514–549, 2014.

A. A. Gavrilov and A. V. Shebelev. Single-fluid model of a mixture for laminar flows of highly concentrated suspensions. Fluid Dynamics, 53(2):255–269, 2018.

Andrés L. Granados. Reynolds transport theorems and conservation principles as special applications of leibniz rule. In Proceedings of the Third Caribbean Congress on Fluid Dynamics, volume III, Universidad Simon Bolivar, Caracas, Venezuela, 1995.

Elisabeth Guazzelli and Olivier Pouliquen. Rheology of dense granular suspensions. Journal of Fluid Mechanics, 852, August 2018.

S. C. Jana, B. Kapoor, and A. Acrivos. Apparent wall slip velocity coefficients in concentrated suspensions of noncolloidal particles. Journal of Rheology, 39(6):1123–1132, November 1995.

D. Monsorno, C. Varsakelis, and M.V. Papalexandris. A two-phase thermomechanical theory for granular suspensions. Journal of Fluid Mechanics, 808:410–440, November 2016.

D. Monsorno, C. Varsakelis, and M.V. Papalexandris. *Poiseuille flow of dense non-colloidal suspensions: The role of intergranular and nonlocal stresses in particle migration.* Journal of Non-Newtonian Fluid Mechanics, 247:229–238, August 2017.

Jeffrey F. Morris and Fabienne Boulay. Curvilinear flows of noncolloidal suspensions: The role of normal stresses. Journal of Rheology, 43(5):1213–1237, 1999.

Ch. B. Narmuratov and A. S. Solov'ev. Effect of suspended particles on the stability of plane poiseuille flow. Fluid Dynamics, 21:38–44, January 1986.

Bastian E. Rapp. Fluids. In Microfluidics: Modeling, Mechanics and Mathematics, chapter 9. Elsevier, 2017.

Rafael G. Henríquez Rivera, Xiao Zhang, and Michael D. Graham. Mechanistic theory of margination and flow-induced segregation in confined multicomponent suspensions: Simple shear and poiseuille flows. Physical Review Fluids, 1, October 2016.

Alexandros Savvides. Chapter 1: Introduction. University of Cyprus, Department of Life and Health Sciences, 2023. URL https://www.ucy.ac.cy/mas/wp-content/uploads/sites/46/2023/05/Introduction_Alexandros_Savvides_2023.pdf.

SimScale. Cfd numerics: Relaxation factors, September 2025. URL https://www.simscale.com/docs/simulation-setup/numerics/relaxation-factors/.

Taha Sochi. Slip at fluid-solid interface. Polymer Reviews, 51(4):309–340, January 2011.

C. Varsakelis, V. Gelbgras, and M.V. Papalexandris. *On the wall boundary condition for the velocity in concentrated suspensions.* Journal of Non-Newtonian Fluid Mechanics, 305, July 2022.

J. Xu, C. Yang, Y.J. Sheng, and H.K. Tsao. Apparent hydrodynamic slip induced by density inhomogeneities at fluid-solid interfaces. Soft Matter, 11(35):6916–6920, 2015.

Kyongmin Yeo and Martin R. Maxey. Numerical simulations of concentrated suspensions of monodisperse particles in a poiseuille flow. Journal of Fluid Mechanics, 682:491–518, 2011.

UNIVERSITÉ CATHOLIQUE DE LOUVAIN
École polytechnique de Louvain
Rue Archimède, 1 bte L6.11.01, 1348 Louvain-la-Neuve, Belgique | **www.uclouvain.be/epl**